




Article

Mitigating Microbiologically Influenced Corrosion of Iron Caused by Sulphate-Reducing Bacteria Using ZnO Nanoparticles

Harith Ambepitiya ¹, Supun Rathnayaka ¹, Yashodha Perera ¹, Chamindu Jayathilake ¹, Himashi Ferdinandez ¹, Ajith Herath ² , Udul Sanjula ², Aishwarya Rathnayake ², Charitha Basnayaka ^{1,*}  and Eustace Fernando ^{1,*} 

¹ Department of Biology, Faculty of Applied Sciences, Rajarata University, Mihintale, Anuradhapura 50300, Sri Lanka; harithambepitiya99@gmail.com (H.A.); supunslbrathnayaka@gmail.com (S.R.); yasodhawajiramali@gmail.com (Y.P.); chamijayathilake1@gmail.com (C.J.); himashi@as.rjt.ac.lk (H.F.)

² Department of Chemical Sciences, Faculty of Applied Sciences, Rajarata University, Mihintale, Anuradhapura 50300, Sri Lanka; ajithch037@gmail.com (A.H.); sanjulachemrc6@gmail.com (U.S.); aishwaryarathnayake@gmail.com (A.R.)

* Correspondence: charitha@as.rjt.ac.lk (C.B.); eustace6192@as.rjt.ac.lk (E.F.); Tel.: +94-7-1459-0499 (C.B.); +16-0-9721-9438 (E.F.)

Abstract

Microbiologically Influenced Corrosion (MIC) significantly endangers steel infrastructure, particularly in marine and buried environments, causing considerable economic and environmental damage. Sulphate-reducing bacteria (SRB) are primary supporters of MIC, accelerating iron corrosion through hydrogen sulfide production. Conventional mitigation strategies, including protective coatings and cathodic protection, often face challenges such as limited effectiveness against SRB and the aggressiveness of saltwater corrosion. This study explores a novel approach by directly introducing zinc oxide (ZnO) nanoparticles into the microbial medium to inhibit SRB activity and reduce MIC. Iron metal coupons were immersed in seawater under three conditions: control (seawater only), seawater with SRB, and SRB with ZnO nanoparticles. These coupons were used as electrodes in microbial fuel cells to obtain real-time voltage readings. At the same time, corrosion was evaluated using cyclic voltammetry (CV), scanning electron microscopy (SEM), energy-dispersive X-ray spectroscopy (EDX), mass loss, and pH measurements. Results demonstrate that ZnO nanoparticles significantly inhibited SRB growth, as confirmed by the antibiotic susceptibility test (ABST). It was revealed that the corrosion rate increased by 21.3% in the presence of SRB compared to the control, whereas the ZnO-added electrode showed a 21.7% reduction in corrosion rate relative to the control. SEM showed prominent corrosive products on SRB-exposed coupons. ZnO-added coupons exhibited a protective layer with grass-like whisker structures, and EDX results confirmed reduced sulfur and iron sulfide deposits, indicating suppressed SRB metabolic activity. ABST confirmed ZnO's antimicrobial properties by producing clear inhibition zones. ZnO nanoparticles offer the dual benefits of antimicrobial activity and corrosion resistance by forming protective self-coatings and inhibiting microbial growth, making them a scalable and eco-friendly alternative to traditional corrosion inhibitors. This application can significantly extend the lifespan of iron structures, particularly in environments prone to microbial corrosion, demonstrating the potential of nanomaterials in combating microbiologically influenced corrosion (MIC).

Keywords: microbiologically influenced corrosion (MIC); sulphate-reducing bacteria (SRB); zinc oxide nanoparticles (ZnO); iron corrosion; corrosion mitigation



Academic Editor: Tao Sun

Received: 25 August 2025

Revised: 6 October 2025

Accepted: 9 October 2025

Published: 11 October 2025

Citation: Ambepitiya, H.; Rathnayaka, S.; Perera, Y.; Jayathilake, C.; Ferdinandez, H.; Herath, A.; Sanjula, U.; Rathnayake, A.; Basnayaka, C.; Fernando, E. Mitigating Microbiologically Influenced Corrosion of Iron Caused by Sulphate-Reducing Bacteria Using ZnO Nanoparticles. *Processes* **2025**, *13*, 3239. <https://doi.org/10.3390/pr13103239>

Copyright: © 2025 by the authors. Licensee MDPI, Basel, Switzerland. This article is an open access article distributed under the terms and conditions of the Creative Commons Attribution (CC BY) license (<https://creativecommons.org/licenses/by/4.0/>).

1. Introduction

Microbiologically Influenced Corrosion (MIC) is a complex phenomenon in which microorganisms alter electrochemical reactions at the metal interface, either accelerating or inhibiting metal corrosion. This process involves microbial stimulation of cathodic or anodic reactions or the creation of differential oxygen concentration cells within confined electrolytic environments [1,2]. The formation of microbial biofilms and associated bacterial activity beneath these films strongly influence MIC [3]. MIC results from the interaction among bacteria, the surrounding medium, and the metal substrate and can be classified as aerobic or anaerobic [3].

Microorganisms induce localized corrosion effects, including pitting, erosion-corrosion, dealloying, stress corrosion cracking, galvanic corrosion enhancement, and hydrogen embrittlement [4]. The extracellular polymeric substances (EPS) secreted by bacteria facilitate cell attachment and significantly influence electrochemical reactions at the metal–film interface [5]. MIC poses severe challenges across medical implants, oil and gas infrastructure, marine environments, and water systems, with corrosion losses estimated at 20% of global annual corrosion damage, costing trillions in economic terms [6,7].

Steel-based marine engineering facilities are especially vulnerable, facing financial losses, environmental hazards, and safety risks due to corrosion [7]. While conventional coatings mitigate steel corrosion, issues such as toxicity, environmental pollution, and antimicrobial resistance arise from continuous leakage of agents. Intelligent coatings capable of on-demand antibacterial agent delivery and self-healing functionalities, including nanocontainer-based controlled release technologies, are promising emerging solutions [8,9].

MIC biofilms typically comprise diverse microbial consortia synergistically interacting with sessile cells embedded in the biofilm matrix while planktonic cells remain suspended in bulk fluid [10–12]. Under oxygen-rich conditions, the outer regions of biofilms are generally inhabited by aerobic and facultative microorganisms, whereas obligate anaerobes are primarily situated in the deeper layers, where oxygen is mostly absent [13]. The movement of gases and solutes between the biofilm and its external environment is partly influenced by the makeup of the EPS, but is mainly controlled by diffusion or advection, depending on the flow characteristics of the surrounding system [14].

Sulfate-reducing bacteria (SRB) are widely recognized as primary contributors to MIC, particularly in anaerobic sulfate-rich environments, where they generate corrosive iron sulfide deposits [15]. SRB induce corrosion both indirectly through hydrogen sulfide production and directly via electron withdrawal by metabolic coupling [16]. Although iron sulfide formation sometimes mitigates or exacerbates corrosion, SRB growth in oxygen-depleted moist soils significantly accelerates buried pipeline corrosion [16,17]. The cathodic polarization method's efficacy decreases in SRB presence, but some studies report negligible SRB effect on stress corrosion cracking [18–20]. In addition to SRB, various other microbial groups, including *Enterobacter*, *Pseudomonas*, *Citrobacter*, and *Cronobacter* species, as well as sulfide-oxidizing bacteria (SOB), iron-oxidizing bacteria (IOB), and acid-producing bacteria (APB), have also been implicated in both general and localized microbiologically influenced corrosion (MIC) of carbon steel [11,12].

Electrobiocorrosion is influenced by environmental factors such as nitrate, Fe(III), and carbon dioxide; nevertheless, sulfate reducers like *Desulfovibrio* species remain closely linked to intense anaerobic corrosion [21,22]. The anodic reaction involves metal oxidation ($\text{Fe} \rightarrow \text{Fe}^{2+} + 2\text{e}^{-}$), while the cathodic reaction involves electron consumption ($2\text{e}^{-} + 2\text{H}^{+} \rightarrow \text{H}_2$). Electrochemical techniques measure corrosion rates in microbial presence; however, external electric fields and media components like yeast extract can influence biofilm activity, complicating interpretation [23].

Metal oxide nanoparticles are of particular interest in materials research due to their diverse mechanical, structural, thermal, electronic, magnetic, and optical properties. Among them, zinc oxide (ZnO) nanoparticles have been identified as especially promising, owing to their thermal and mechanical stability at room temperature, good physical and chemical resistance, environmental compatibility, abundant availability, and low cost [24]. Protection strategies commonly employ zinc-based coatings due to their cathodic protection effects, including galvanized steel produced via electrodeposition, hot-dipping, spraying, or thermal diffusion [25].

ZnO nanoparticles have been continuously studied as corrosion inhibitors over time. Incorporation of ZnO nanoparticles into coatings enhances steel corrosion resistance by acting as protective barriers [26]. Their integration into nanosilica-containing epoxy formulations has been reported to enhance barrier properties and, consequently, improve corrosion resistance [27]. In addition, epoxy resins with different ZnO nanofillers, including commercial, recycled, and functionalized ZnO nanoparticles, exhibited increased corrosion resistance in ZnO-epoxy composites, suggesting that the type of nanofiller influences protective performance [28]. Moreover, ZnO/polymer nanocomposites demonstrated protective performance for mild steel in 5% HCl solution, indicating effectiveness under acidic conditions [25]. Overall, these studies indicate that integrating ZnO nanoparticles into polymer matrices contributes to improved corrosion protection by enhancing barrier properties, chemical stability, and resistance in aggressive environments.

Inhibition of MIC in marine environments remains a complex task, with current approaches including surface treatments such as physical modification and cathodic protection, the application of protective coatings, material design through antibacterial element incorporation and texture tuning, and biological strategies involving EPS interaction, antimicrobial agents, and biomineralization [26]. ZnO-NPs exhibit strong antibacterial activity against both Gram-positive and Gram-negative bacteria, even at low concentrations ranging from 0.16 to 5.00 mmol/L through reactive oxygen species (ROS) generation, membrane disruption, and interference with cellular processes [29,30]. In addition to providing cathodic protection, their broad-spectrum antibacterial properties offer potential for targeting MIC-related microbial populations.

2. Materials and Methods

2.1. Sample Collection and Microorganism Isolation

Marine sediment samples were collected from the Uppuweli coastal area (latitude 8°36'52.92, longitude 81°11'46.67) under sterile conditions to isolate sulfate-reducing bacteria (SRB) [29]. Samples were transported in an ice container and processed within 24 h to ensure microbial viability. SRB isolation was performed using Postgate's B medium [30–32], which supports the growth of sulfate reducers and contains the following components: $\text{MgSO}_4 \cdot 7\text{H}_2\text{O}$ (0.2 g), sodium acetate (CH_3COO^- , 0.1 g), NH_4Cl (0.1 g), CaCl_2 (0.1 g), KH_2PO_4 (0.05 g), Na_2SO_4 (0.1 g), yeast extract (0.1 g), $\text{FeSO}_4 \cdot 7\text{H}_2\text{O}$ (0.05 g), $\text{Na}_2\text{S}_2\text{O}_6$ (0.01 g), and agar (2.5 g) per 100 mL distilled water. The medium was prepared anaerobically by boiling and flushing with nitrogen gas prior to sterilization.

2.2. Molecular Characterization of the Sulfur Reducing Bacterium

Genomic DNA was extracted from the isolated bacterial colonies using a Wizard™ (Promega Corporation, Madison, WI, USA) bacterial genomic DNA extraction kit, as per the manufacturer instructions. The 16s rRNA region was amplified using the universal primer pair 27F and 1492R, according the method and polymerase chain reaction (PCR) conditions described in our earlier studies [33,34]. The amplified PCR products were verified for their size (approximately 1500 bp), and were sequenced using Sanger capillary sequencing

(Macrogen, Seoul, Republic of Korea). The consensus sequences (Contigs) were assembled from trimmed forward and reverse reads using the software BioEdit (Version 7.0.5.3).

Pertaining to the phylogenetic tree, it was inferred using the Maximum Likelihood method and Tamura-Nei (1993) model [35] of nucleotide substitutions and the tree with the highest log likelihood (−1686.61) is shown. The tree is drawn to scale with branch lengths (shown next to the branches) computed using the Maximum Likelihood method [36] and measured in the number of substitutions per site. The percentage of replicate trees in which the associated taxa clustered together (2500 replicates) is shown next to the branches [37]. Initial tree(s) for the heuristic search were obtained automatically by applying Neighbor-Joining [38] and BioNJ [39] algorithms to a matrix of pairwise distances estimated using the Maximum Composite Likelihood (MCL) [40] approach, and then selecting the topology with superior log likelihood value. The analytical procedure encompassed 8 nucleotide sequences. The complete deletion option was applied to eliminate positions containing gaps and missing data resulting in a final data set comprising 726 positions. Evolutionary analyses were conducted in MEGA version 12 molecular evolutionary genetics software [41].

2.3. Preparation of Artificial Seawater Medium (ATSM) and Gas-Absorbent Sachets

Artificial seawater medium (ATSM) was prepared to simulate the marine ionic composition [42], containing NaCl (24.53 g/L), MgCl₂ (5.20 g/L), Na₂SO₄ (4.09 g/L), CaCl₂ (1.16 g/L), KCl (0.695 g/L), NaHCO₃ (0.201 g/L), and KBr (0.101 g/L). Gas-absorbent sachets composed of NaBH₄ (1 g), NaHCO₃ (0.5 g), citric acid (1 g), and CoCl₂ (1 g) were used to maintain anaerobic conditions within the microbial fuel cell chambers.

2.4. Synthesis and Characterization of ZnO Nanoparticles

ZnO nanoparticles were synthesized via a chemical precipitation method adapted from [43]. Zinc acetate dihydrate was dissolved in distilled water, and sodium hydroxide solution was slowly added under constant stirring at room temperature, resulting in the formation of ZnO precipitates. The precipitates were washed, dried, and calcined at 40 °C for 3 h. Nanoparticles were characterized by Scanning Electron Microscopy (SEM; model and manufacturer), dynamic light scattering (DLS; model and manufacturer), and zeta potential measurements to confirm particle size distribution, morphology, and colloidal stability.

2.5. Microbial Fuel Cell (MFC) Setup

A dual-chamber microbial fuel cell was constructed using acrylic chambers separated by a proton exchange membrane (Nafion 117, Dual Dispersion Technologies, Bedford Hills, NY, USA). Carbon electrodes initially served as an anode and a cathode. After establishing a stable microbial community, carbon anodes were replaced with pre-cleaned iron coupons (dimension: 1 cm × 1 cm × 1 cm). The anode chamber was inoculated with isolated SRB in ATSM under anaerobic conditions ensured by gas-absorbent sachets and nitrogen flushing. The cathode chamber contained ATSM and 100 mM potassium ferricyanide as an electron acceptor. The system was maintained at 30 °C in an incubator throughout the experiment duration (14 days). Voltage and current were measured across external resistors using a PicoLog™ 1012 data logger at 30 s intervals. The MFC was set up according to [33,34].

2.6. Electrochemical Measurements

Electrochemical behavior was assessed by cyclic voltammetry (CV) using a CHI 9201D electrochemical workstation (CH Instruments, Austin, TX, USA). Iron electrodes acted as working electrodes, a platinum wire as auxiliary electrode, and an Ag/AgCl (1 M KCl) electrode as reference. Measurements were conducted in an ATSM electrolyte under ambient temperature. Initial voltammograms were recorded for ATSM alone,

followed by electrodes exposed to SRB and SRB + ZnO nanoparticles (concentration: X mg/L). Scan rates and potential ranges were optimized based on preliminary tests (e.g., 10–100 mV/s, −0.5 to +0.5 V vs. Ag/AgCl). Ohm's law ($I = V/R$) was applied to calculate current from voltage data [44].

2.7. Surface Morphology and Elemental Analysis

Post-experimental iron electrodes were gently rinsed with sterile distilled water and dried under nitrogen gas. Surface morphology and biofilm presence were examined using a Carl Zeiss EVO 18 (Oberkochen, Germany) microscope with an optical magnification range of 20–135 \times , an electron magnification range of 100 \times –10,000 \times , a maximal digital zoom of 12 \times , an acceleration voltage of 10 kV (Figures S1–S6). Elemental composition and corrosion product identification were performed using Energy Dispersive X-ray Spectroscopy (EDS) attached to the SEM system (Figures S7–S9). Multiple spots per electrode were analyzed to ensure representative data. Paraffin oil residues, used for sample storage, were considered in elemental interpretation to avoid confounding artifacts.

2.8. Corrosion Rate Determination

Corrosion rates were evaluated via mass loss measurements. Iron electrodes were weighed using an analytical balance (precision ± 0.1 mg) before and after the 14-day exposure to experimental conditions. Electrodes were cleaned following ASTM G1-03 (2017) standards to remove corrosion products without metal loss [45]. Corrosion rate was calculated using the formula:

$$\text{Corrosion Rate} = \Delta m / (A \times t \times \text{density})$$

where Δm = weight loss (g), A = exposed surface area (cm^2), and t = exposure time (hours). Data were averaged from triplicate samples per treatment group.

2.9. Antibiotic Susceptibility Testing of Isolated Microorganisms

Isolated bacterial cultures were tested for susceptibility to ZnO nanoparticles using well diffusion assays on Postgate's B agar plates inoculated with bacterial suspensions standardized to 0.5 McFarland turbidity. Wells were bored into the agar spread plates of bacterial cultures using a sterile cork borer. ZnO nanoparticles were impregnated into wells (0.1 M concentration) thereafter, and zones of inhibition were measured after 48 h anaerobic incubation at 30 °C, following CLSI guidelines (<https://clsi.org/shop/standards/m100/>, accessed on 18 August 2025).

3. Results

3.1. Initial Microbial Community Stability

The carbon electrodes in the microbial fuel cells (MFCs) were connected to an external resistor, and stable, maximal voltage output was observed after approximately five days, indicating that the microbial community had reached electrochemical equilibrium. Voltage profiles recorded via the PicoLog™ 1012 data logger showed consistent patterns corresponding to nutrient availability: voltage decreased when nutrients were depleted and increased upon refeeding, stabilizing for at least 24 h. This reproducible response confirmed that the microbial community was metabolically active and responsive to environmental changes. Since the system operated under constant external resistance, voltage changes correlated directly with current changes following Ohm's Law. The electrical stability demonstrated adaptation and sustained electron transfer capability of the electroactive microbial population, confirming its suitability for corrosion studies. Initial SRB enrichment was performed using Postgate's B medium supplemented with L-cysteine, which enhanced

anaerobic conditions and facilitated SRB growth, evidenced by red and black precipitates, sulfide odor, and colonies formed after 3–5 days. A mixed SRB consortium was obtained via the pour plate method, and pure cultures were isolated by streaking colonies on fresh agar plates, resulting in distinct colonies in Figure 1.

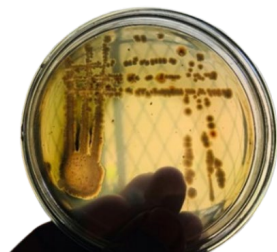


Figure 1. Streak plate with isolated bacterial colonies isolated from the MFC system.

3.2. Electrochemical Characterization: Current vs. Voltage Plot

The current (amperes) versus voltage (volts) plot showed a nonlinear relationship between current and voltage, with voltage ranging up to 100 V. This suggests complex electrochemical behaviour beyond simple ohmic conduction in the system in Tables 1–3, Figures 2–4.

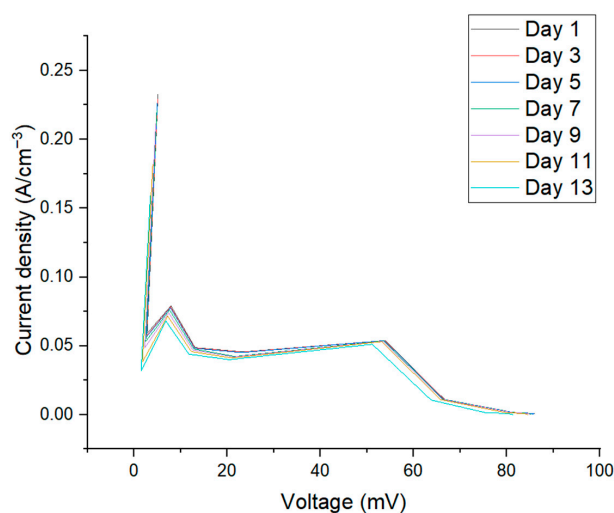


Figure 2. Temporal changes in current density vs. voltage in the control setup over 13 days.

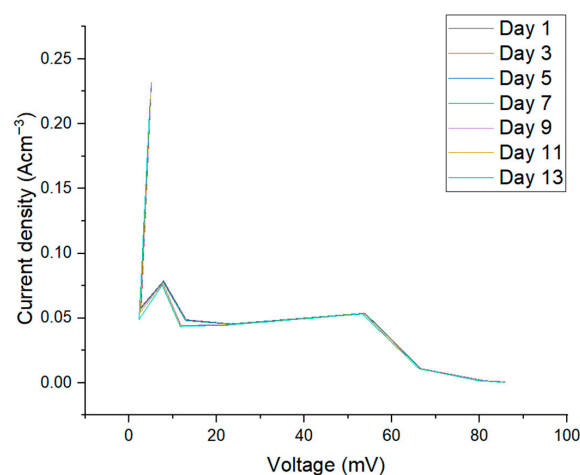


Figure 3. Temporal changes in current density vs. voltage in the isolated bacterium + No ZnO over 13 days.

Table 1. Control setup voltages against resistance.

R (Om)	Date	Day1	Day3	Day5	Day7	Day9	Day11	Day13
	Voltage (mV)							
22		5.12	5.04	4.98	4.86	4.65	4	3.5
41		2.78	2.7	2.65	2.5	2.29	1.8	1.5
100		7.91	7.83	7.77	7.61	7.4	7.17	6.8
268		13.08	13	12.94	12.8	12.59	12.3	11.78
510		23.25	23.17	23	21.6	21.39	21.01	20.42
1000		53.88	53.8	53.74	53.58	53.37	53.08	51.12
6000		66.67	66.59	66.51	66.35	66.14	65.8	63.76
47,000		81.32	81.24	81.18	81.02	80.77	79.5	75.32
100,000		85.91	85.84	85.78	84.92	84.66	83.78	80.52
1,000,000		85.56	85.48	85.42	85.26	85	84.6	81.33

Table 2. ATSM + isolated bacterium setup voltages against resistance.

R (Om)	Date	Day1	Day3	Day5	Day7	Day9	Day11	Day13
	Voltage (mV)							
22		5.1	5.07	5.04	4.99	5	4.9	4.75
41		2.76	2.73	2.7	2.65	2.65	2.55	2.3
100		7.89	7.86	7.83	7.78	7.73	7.64	7.54
268		13.06	13.03	12.99	12.86	11.9	11.79	11.68
510		23.23	23.2	23.17	23.09	22.92	22.83	22.73
1000		53.86	53.82	53.79	53.74	53.5	53.41	53.2
6000		66.65	66.61	66.57	66.52	66.4	66.33	66.12
47,000		81.3	81.26	81.22	81.17	81	79.98	79.75
100,000		85.89	85.84	85.81	85.76	85.5	84	83.79
1,000,000		85.54	85.5	85.47	85.42	85.32	85.11	84.9

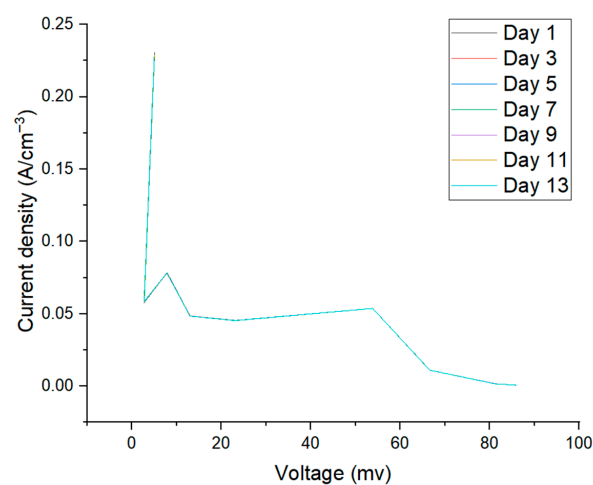
**Figure 4.** Temporal changes in current density vs. voltage in the isolated bacterium + ZnO over 13 days.

Table 3. ATSM + isolated bacterium + ZnO setup voltages against resistance.

R (Om)	Date	Day1	Day3	Day5	Day7	Day9	Day11	Day13
	Voltage (mV)							
22		5.07	5.02	5.03	5.01	5.02	5.04	5
41		2.73	2.71	2.72	2.7	2.73	2.75	2.76
100		7.86	7.83	7.84	7.83	7.8	7.83	7.84
268		13.03	13.01	13	13.02	13.05	13	12.98
510		23.2	23.17	23.19	23.17	23.13	23.12	23.11
1000		53.83	53.82	53.83	53.84	53.82	53.83	53.82
6000		66.62	66.6	66.6	66.6	66.58	66.57	66.58
47,000		81.27	81.25	81.27	81.28	81.3	81.27	81.25
100,000		85.86	85.84	85.83	85.81	85.83	85.85	85.86
1,000,000		85.51	85.49	85.51	85.52	85.53	85.52	85.53

3.3. Electrochemical Characterization of Metal Electrodes Using Cyclic Voltammetry (CV)

In cyclic voltammetry experiments with corroded Fe electrodes as working electrodes in ATSM electrolyte, the voltammogram showed a broad current response without distinct redox peaks, indicating no clear electrochemical reactions within the scanned potential range. This phenomenon was attributed to the formation of a passivating corrosion layer composed of iron oxides or hydroxides, and nonspecific background currents induced by seawater ions contributed to capacitive behavior rather than Faradic electrochemical processes (Figure 5). When ZnO nanoparticles were added to the electrolyte with isolated bacterium inoculated Fe electrodes, the voltammogram showed a narrower and clearer window. The presence of ZnO inhibited isolated bacterium activity, reducing biofilm formation and suppressing formation of SRB-related corrosion products, thereby improving the electrochemical response and electrode surface condition (Table 4). This was observed as a shift from a flat, passive voltammogram to a more active one with distinct electrochemical features (Figure 6).

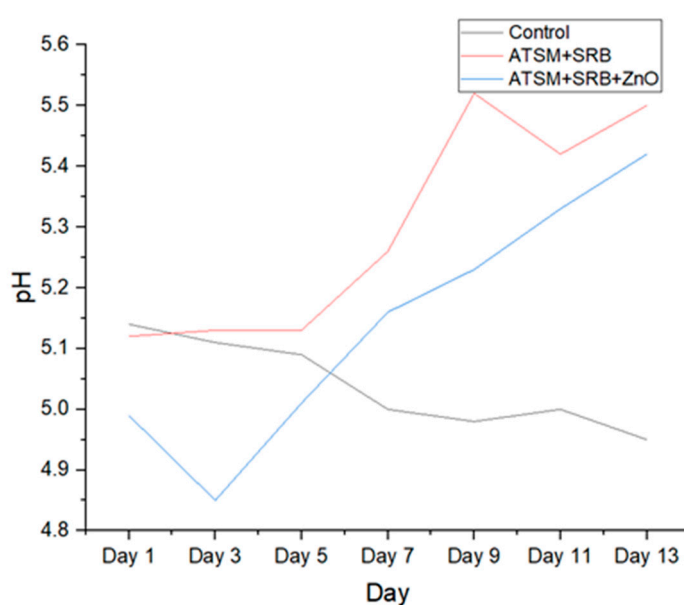
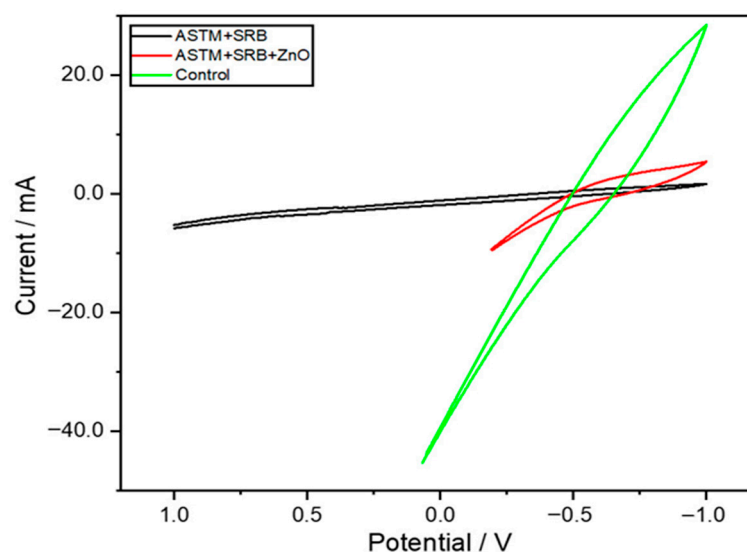
**Figure 5.** Temporal changes in pH within the system over a period of 13 days.

Table 4. Temporal pH differences in microbial fuel cells.

Date	Control	ATSM + Isolated Bacterium	ATSM + Isolated Bacterium + ZnO
01/10	5.14	5.12	4.99
01/12	5.11	5.13	4.85
01/14	5.09	5.13	5.01
01/16	5	5.26	5.16
01/18	4.98	5.52	5.23
01/20	5	5.42	5.33
01/22	4.95	5.5	5.42

**Figure 6.** Cyclic Voltammograms of the ASTM + SRB (isolated bacterium), ASTM + SRB (isolated bacterium) + ZnO experiments compared to the control experiment.

3.4. Characterization of Surface Morphology and Corrosion Analysis by Scanning Electron Microscopy

SEM analysis revealed that electrodes treated with isolated bacterium plus ZnO nanoparticles exhibited significantly reduced corrosion compared to electrodes treated with isolated bacterium alone or control samples. Although some corrosion and deposits were present, their extent was visibly less in the ZnO-treated group, indicating that ZnO nanoparticles exerted an inhibitory effect on isolated bacterium activity or altered the corrosion mechanism, providing partial protection against corrosion (Figure 7a–c).

3.5. Identification and Quantification of Elemental Composition of Electrodes Using Energy Dispersive X-Ray Spectroscopy (EDS)

EDS analysis of SRB-treated electrodes without ZnO showed that iron constituted approximately 80% of the electrode surface, with carbon content ranging between 3% and 5%, and silicon between 1% and 3%, likely reflecting corrosion products and microbial biofilm deposits on the electrode surface (Figure 7d).

3.6. Mass Loss Observations and Corrosion Rate Calculation

Mass loss measurements showed slight weight changes in electrodes over the 14-day period control electrodes lost 0.0014 g, isolated bacterium-treated electrodes lost 0.0017 g, and ZnO + isolated bacterium-treated electrodes lost 0.0011 g. Corresponding corrosion

rates were 0.0465 mm/year for control, 0.0565 mm/year for isolated bacterium-treated, and 0.0365 mm/year for ZnO + isolated bacterium-treated electrodes. The increased corrosion rate with isolated bacterium reflects microbiologically influenced corrosion via sulfide formation (Figure 8). The decreased corrosion rate in ZnO treated electrodes (21.7% lower than control) suggests that ZnO nanoparticles provided a protective effect, likely by forming a surface layer inhibiting isolated bacterium colonization and corrosion, as supported by SEM observations of a grassland-like morphology attributed to ZnO nanoparticle adhesion (Table 5).

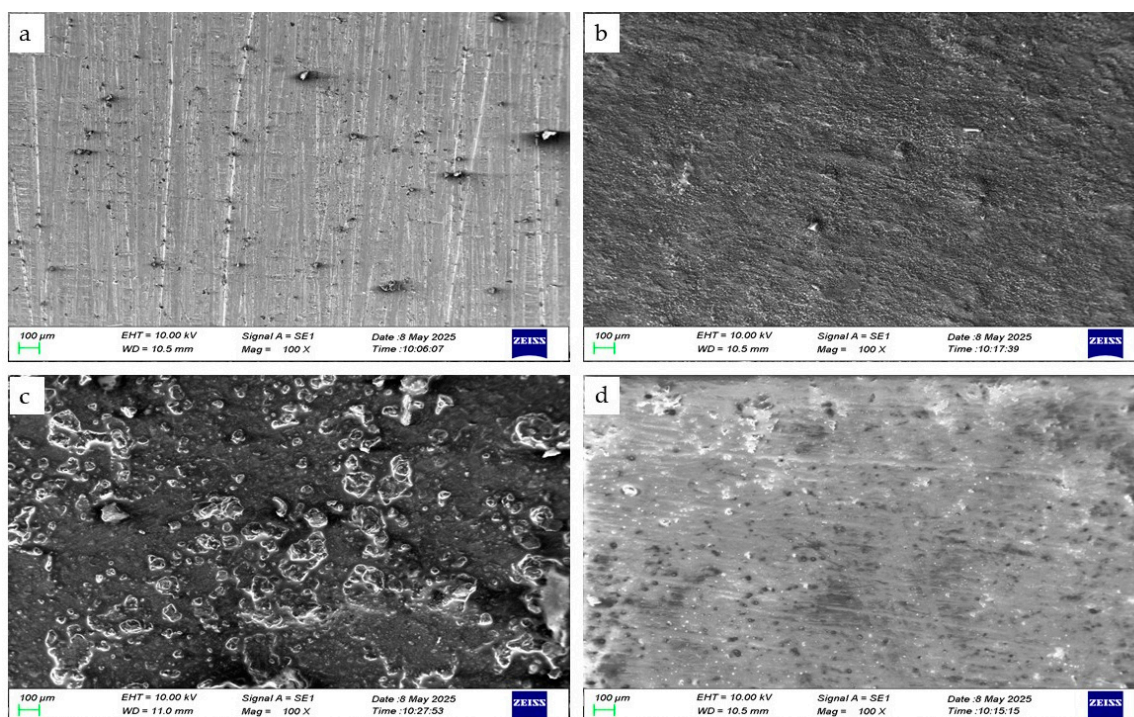


Figure 7. (a) 100× untreated polished (bare) metal surface, (b) 100× electrode exposed to isolated microorganism showed clear signs of corrosion, (c) 5000× ATSM + isolated microorganism + ZnO electrode surface, (d) 100× electrode exposed to ZnO.

Table 5. Mass loss observations of electrodes.

Electrode	Initial Weight (g)	Final Weight (g)	Difference (g)
Control	3.6984	3.6998	0.0014
Isolated bacterium	3.7029	3.7046	0.0017
ZnO + isolated bacterium	3.7123	3.7134	0.0011

3.7. Molecular Characterization of Isolated Microorganisms

According to 16srRNA-based molecular analysis and BLAST analysis (National Center for Biotechnology Information (NCBI) website), this sulfur-reducing bacterium was closely related to *Enterobacter cloacae* (with a 100% identity). The 16S rRNA gene marker based phylogenetic tree in Figure 9 revealed that, this bacterium clusters with *Enterobacter cloacae* strains NBRC 13535 and DSM 30054 with 98% bootstrap value.

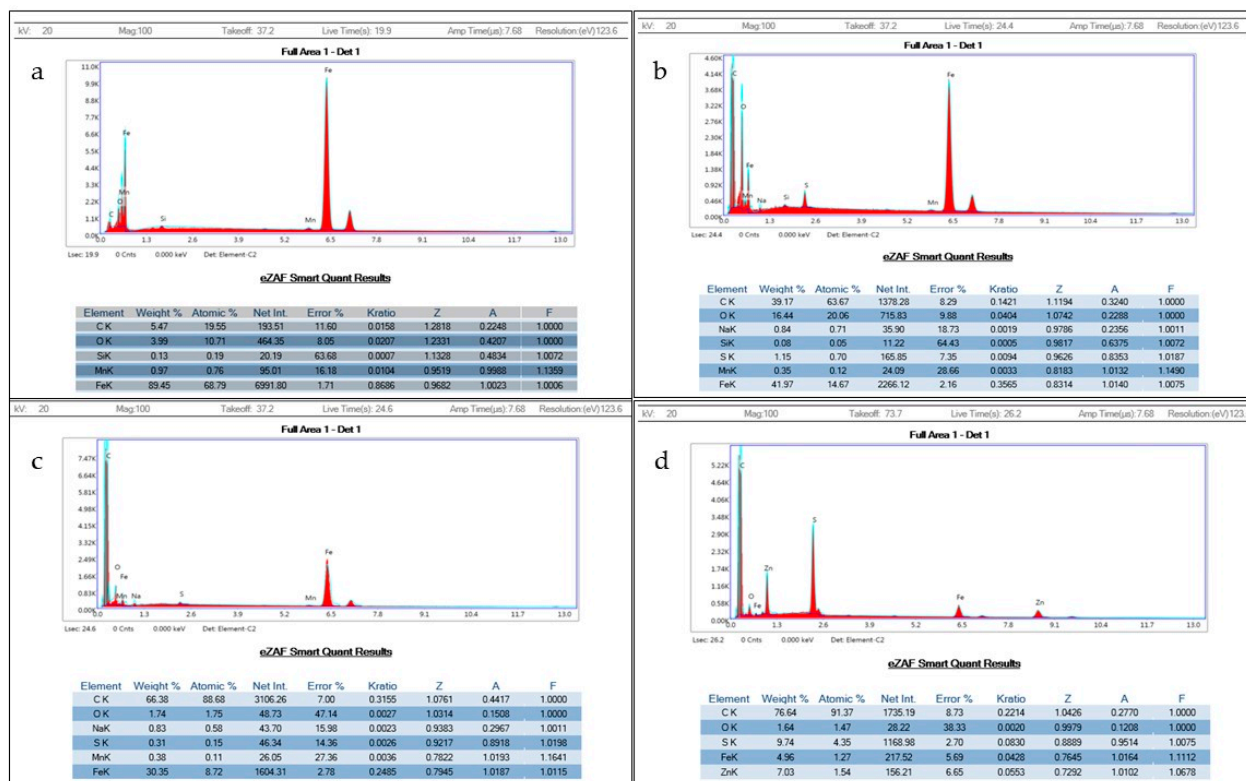


Figure 8. Corresponding electrode elemental composition of electrodes using Energy Dispersive X-ray Spectroscopy of (a) untreated polished (bare) metal surface, (b) electrode exposed to isolated microorganism, (c) ATSM + isolated microorganism + ZnO electrode surface, (d) electrode exposed to ZnO.

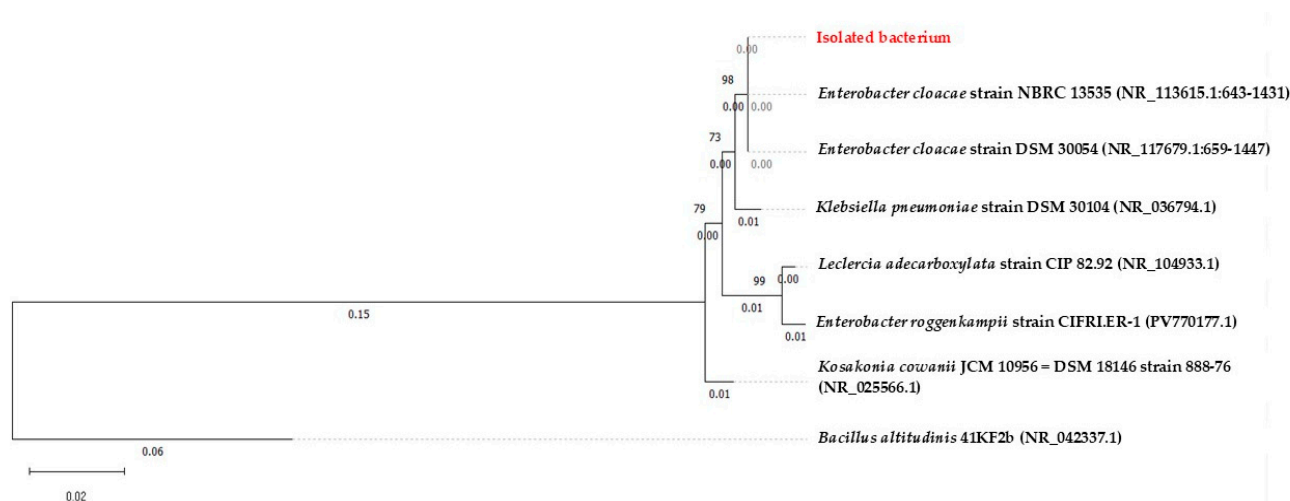


Figure 9. Phylogenetic tree constructed with 16S rRNA-based molecular analysis.

3.8. Antibiotic Susceptibility Test of Isolated Microorganisms Against ZnO Nanoparticles

ZnO nanoparticles inhibit the growth of isolated microorganisms, contributing to corrosion mitigation (Figure 10).

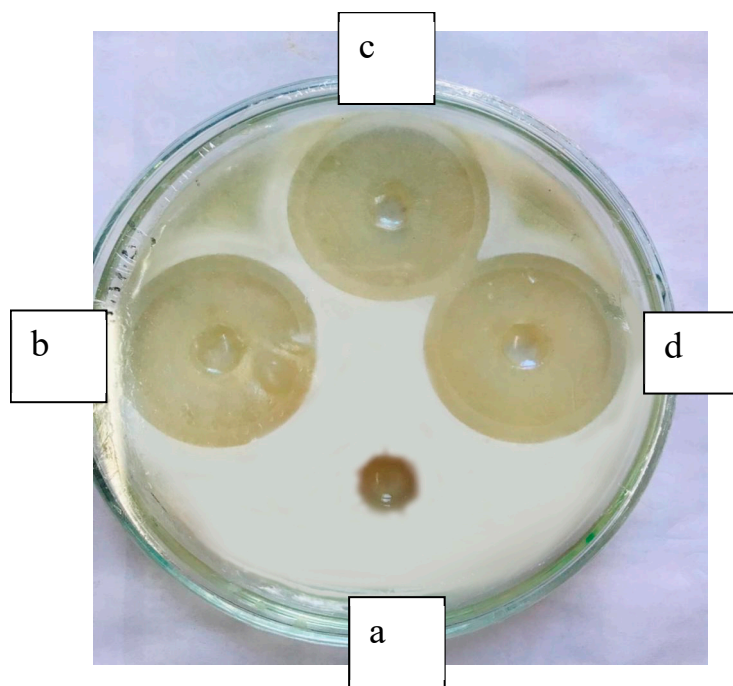


Figure 10. Antibiotic susceptibility test of isolated microorganisms against ZnO nanoparticles. Inhibition zone shown with label-a, is the control experiment with sterile distilled water and inhibition zones shown in labels b, c and d are replicates of the same ZnO nanoparticles concentration (0.1 M) loaded onto the wells.

4. Discussion

The initial microbial community stability in the MFCs was confirmed by stable voltage profiles over days, emphasizing the successful establishment of an electroactive biofilm adapted for sustainable electron transfer. The use of Postgate's B medium with L-cysteine fostered effective SRB growth under anaerobic conditions, corroborated by characteristic sulfide precipitates and colony morphology, facilitates further corrosion studies.

The stable voltage and current across multiple external resistances affirm that the microbial consortium was functionally active and electronically integrated with the electrodes. This stability is critical for reliable investigation of biocorrosion mechanisms and protective interventions.

The pH trends highlight the dynamic biochemical processes involved. The initial acidification in the ZnO + isolated bacterium setup is likely due to ZnO dissolution, which releases protons, or early SRB metabolic activity, generating acidic intermediates. The subsequent alkalization suggests that active SRB metabolism eventually dominated, producing sulfide ions and other alkaline substances that neutralized acidity. This interplay underscores the important role ZnO nanoparticles play in modifying the local chemical environment, potentially influencing microbial growth and corrosion pathways.

Electrochemical characterization through CV revealed the inhibitory effect of corrosion layers in the control electrode, while ZnO nanoparticles improved electrochemical response, likely by limiting the development and preventing thick passivating corrosion products typically caused by SRB activity. The improved voltammetric features after ZnO treatment suggest a shift towards more reversible redox processes, corroborating the observed reduction in corrosion. The cyclic voltammetry (CV) profiles obtained from corroded Fe electrodes immersed in ATSM electrolyte revealed a broad, featureless current response devoid of distinct redox peaks. This electrochemical signature is characteristic of a surface dominated by non-Faradaic processes, primarily capacitive charging and discharging. The

absence of well-defined redox transitions suggests that the electrode surface is covered by a passivating layer composed of iron oxides (Fe_2O_3 , Fe_3O_4) and hydroxides, which impede electron transfer and suppress electrochemical activity. Additionally, the presence of seawater-derived ions (Cl^- , SO_4^{2-} , Mg^{2+} , Na^+) contributes to diffuse background currents, further masking any underlying Faradaic reactions and reinforcing the capacitive nature of the voltammogram.

Upon inoculation with isolated bacterium, the electrochemical environment becomes more aggressive due to the microbial reduction of sulphates to hydrogen sulfide (H_2S), which accelerates iron dissolution and promotes the formation of poorly conductive iron sulfide layers. These bio-corrosion products exacerbate surface passivation and further flatten the voltammetric response.

However, the introduction of ZnO nanoparticles into the isolated bacterium-inoculated system induces a marked transformation in the voltammetric profile. The CV curves exhibit a narrower potential window with more defined electrochemical features, indicating a partial restoration of Faradaic activity. This improvement is attributed to the antimicrobial action of ZnO nanoparticles, which inhibit isolated bacterium metabolism and biofilm formation. By suppressing the generation of H_2S and limiting the deposition of iron sulfides, ZnO preserves the integrity of the Fe surface and reduces the extent of passivation.

Moreover, ZnO's amphoteric behavior contributes to localized pH elevation, creating an alkaline microenvironment that further inhibits SRB activity and promotes the formation of stable iron oxide layers with improved electrochemical accessibility. The emergence of redox peaks or increased current density in the modified voltammogram reflects enhanced charge transfer kinetics and improved surface reactivity, underscoring the dual role of ZnO nanoparticles in microbial suppression and electrochemical stabilization.

This shift from a flat, passive voltammogram to a more active and structured profile provides compelling electrochemical evidence of ZnO's efficacy in mitigating MIC and restoring electrode functionality [46].

SEM analysis further supported the protective role of ZnO, showing reduced surface damage, which is consistent with the reduced corrosion rates measured. The formation of "grassland"-like whisker structures on the ZnO-treated electrode surfaces indicates nanoparticle adhesion, creating a physical barrier against SRB colonization and corrosive byproduct formation. In this study, ZnO nanoparticles were synthesized via low-temperature calcination at 40°C , which is significantly below the conventional range of $300\text{--}600^\circ\text{C}$ typically required for forming well-crystallized ZnO from zinc acetate. As XRD analysis was not available to confirm crystallinity, the presence of Zn was verified using SEM and EDX techniques. EDX spectra confirmed elemental zinc distribution, supporting successful nanoparticle formation, although the low calcination temperature may have resulted in amorphous or poorly crystalline ZnO. According to [47], crystalline ZnO nanoparticles could be synthesized at 40°C , exhibiting wurtzite crystal structures, as confirmed by XRD analysis. At this mild temperature, nanoparticles typically present sizes from 8 to 45 nm with spherical and rod morphologies. Controlled pH and precursor reactions drive nucleation and crystallization, even under low-thermal-energy conditions.

The corrosion rates quantitatively confirmed that isolated bacterium promote enhanced corrosion due to sulfate reduction and sulfide formation, while ZnO nanoparticles significantly mitigated these effects, reducing corrosion by about 22% compared to the control. This protective effect of ZnO may surround antibacterial action against SRB and alteration of surface chemistry, representing a promising biocorrosion control strategy.

The addition of ZnO nanoparticles to aqueous systems markedly increases local pH due to their amphoteric nature and surface reactivity. Upon hydrolysis, ZnO releases hydroxide ions and adsorbs protons, creating an alkaline environment that disrupts the

metabolic activity of SRB, which prefer mildly acidic conditions. This pH shift not only inhibits microbial production of corrosive hydrogen sulfide, but also promotes the passivation of iron surfaces via stable oxide layer formation. Together, these effects highlight ZnOs dual role in microbial suppression and corrosion resistance, positioning it as a sustainable alternative to conventional inhibitors [48,49].

Molecular characterization underlined the microbial diversity involved with *Enterobacter cloacae* identified among isolates, which may contribute to corrosion dynamics. The antibiotic susceptibility tests on ZnO nanoparticles emphasize the multifunctional role of ZnO beyond passive surface protection, potentially acting as an antimicrobial agent against corrosion-inducing microbes.

Enterobacter cloacae has been identified as a anaerobic bacterium with sulphate reducing ability. According to [50], *E. cloacae* has a complex sulfate reduction mechanism with the help of encoded enzymes for both assimilatory and dissimilatory sulfate reduction pathways. *E. cloacae* differed from strict anaerobic SRB by being able to tolerate oxygen while maintaining sulfate-reduction capabilities, making these bacteria potentially important in industrial and environmental settings, such as bioremediation and microbial corrosion control.

5. Conclusions

This study successfully demonstrates that ZnO nanoparticles serve as an effective and eco-friendly inhibitor of MIC of iron, specifically against non-classic SRB. The incorporation of ZnO nanoparticles into the microbial medium significantly suppressed SRB metabolic activity and biofilm formation, as evidenced by antibiotic susceptibility tests, reduced sulfur deposits in EDX analysis, and diminished surface degradation observed via SEM. Electrochemical and mass loss measurements quantitatively confirmed that ZnO treatment reduced the corrosion rate by 21.7% compared to the control, effectively counteracting the 21.3% increase in corrosion induced by SRB. The nanoparticles not only exhibited strong antimicrobial properties, but also contributed to the formation of a protective surface layer, enhancing corrosion resistance. These results highlight the dual functionality of ZnO nanoparticles as both a microbial inhibitor and a corrosion mitigant, offering a scalable, sustainable, and practical alternative to conventional corrosion protection methods in marine and industrial environments prone to MIC.

Supplementary Materials: The following supporting information can be downloaded at: <https://www.mdpi.com/article/10.3390/pr13103239/s1>, Figure S1. 100x magnified SRB unexposed metal surface, Figure S2. 100x electrode exposed to ZnO, Figure S3. 250x untreated polished metal surface, Figure S4. 250x control electrode surface, Figure S5. 250x ATSM+SRB electrode surfaces, Figure S6. 10000x ATSM+SRB+ZnO electrode surfaces, Figure S7. Bare metal elemental composition of electrodes using Energy Dispersive X-ray Spectroscopy, Figure S8. Control Setup electrode elemental composition of electrodes using Energy Dispersive X-ray Spectroscopy, Figure S9. Control Setup electrode elemental composition of electrodes using Energy Dispersive X-ray Spectroscopy & SRB+No ZnO treated electrode elemental composition of electrodes using Energy Dispersive X-ray Spectroscopy.

Author Contributions: Conceptualization, C.B. and E.F.; Methodology, C.J., H.F., A.H., U.S. and A.R.; Software, E.F.; Validation, C.B.; Formal analysis, H.A., S.R., Y.P., C.B. and E.F.; Investigation, H.A. and S.R.; Resources, H.F.; Data curation, C.B. and E.F.; Writing—original draft, H.A., S.R. and Y.P.; Writing—review and editing, C.J., H.F., A.H., U.S. and A.R.; Visualization, H.A., S.R. and E.F.; Supervision, C.B. and E.F.; Project administration, C.B. and E.F.; Funding acquisition, C.B. All authors have read and agreed to the published version of the manuscript.

Funding: This research received no external funding.

Data Availability Statement: The original contributions presented in this study are included in the article. Further inquiries can be directed to the corresponding authors.

Conflicts of Interest: The authors declare no conflicts of interest.

Abbreviations

The following abbreviations are used in this manuscript:

MIC	Microbiologically Influenced Corrosion
SRB	Sulphate-Reducing Bacteria
ZnO	Zinc Oxide Nanoparticles
ATSM	Artificial Seawater Medium

References

- Wang, D.; Unsal, T.; Kumseranee, S.; Punpruk, S.; Mohamed, M.E.; Saleh, M.A.; Gu, T. Sulfate reducing bacterium *Desulfovibrio vulgaris* caused severe microbiologically influenced corrosion of zinc and galvanized steel. *Int. Biodeterior. Biodegrad.* **2021**, *157*, 105160. [\[CrossRef\]](#)
- Alasvand Zarasvand, K.; Rai, V.R. Microorganisms: Induction and inhibition of corrosion in metals. *Int. Biodeterior. Biodegrad.* **2014**, *87*, 66–74. [\[CrossRef\]](#)
- Pal, M.K.; Lavanya, M. Microbial Influenced Corrosion: Understanding Bioadhesion and Biofilm Formation. *J. Bio-Tribo-Corros.* **2022**, *8*, 76. [\[CrossRef\]](#)
- Little, B.J.; Lee, J.S. Microbiologically influenced corrosion: An update. *Int. Mater. Rev.* **2014**, *59*, 384–393. [\[CrossRef\]](#)
- Perchikov, R.; Cheliukanov, M.; Plekhanova, Y.; Tarasov, S.; Kharkova, A.; Butusov, D.; Arlyapov, V.; Nakamura, H.; Reshetilov, A. Microbial Biofilms: Features of Formation and Potential for Use in Bioelectrochemical Devices. *Biosensors* **2024**, *14*, 302. [\[CrossRef\]](#)
- Skovhus, T.; Eckert, R.; Rodrigues, E. Management and control of microbiologically influenced corrosion (MIC) in the oil and gas industry—Overview and a North Sea case study. *J. Biotechnol.* **2017**, *256*, 31–45. [\[CrossRef\]](#)
- Gu, T.; Xu, D.; Zhang, P.; Li, Y.; Lindenberger, A. Microbiologically Influenced Corrosion and Its Impact on Metals and Other Materials. *Microbiol. Miner. Met. Mater. Environ.* **2015**, *25*, 383–408.
- Mulijani, S.; Rizky, G.; Wulanawati, A.; Handayani, A.W.; Asih, F.N. Synthesis of zinc oxide nanoparticle as corrosion resistance of steel metal. *AIP Conf. Proc.* **2022**, *2638*, 020006. [\[CrossRef\]](#)
- Sanyal, S.; Park, S.; Chelliah, R.; Yeon, S.-J.; Barathikannan, K.; Vijayalakshmi, S.; Jeong, Y.-J.; Rubab, M.; Oh, D.H. Emerging trends in smart self-healing coatings: A focus on micro/nanocontainer technologies for enhanced corrosion protection. *Coatings* **2024**, *14*, 324. [\[CrossRef\]](#)
- Yang, J.; Wang, Z.; Qiao, Y.; Zheng, Y. Synergistic effects of deposits and sulfate reducing bacteria on the corrosion of carbon steel. *Corros. Sci.* **2022**, *199*, 110210. [\[CrossRef\]](#)
- Agarwal, H.; Gurnani, B.; Pippal, B.; Jain, N. Capturing the micro-communities: Insights into biogenesis and architecture of bacterial biofilms. *BBA Adv.* **2025**, *7*, 100133. [\[CrossRef\]](#)
- Mechmechani, S.; Yammine, J.; Alhuthali, S.; El Mouzawak, M.; Charvourou, G.; Gharsallaoui, A.; Chihib, N.E.; Doulgeraki, A.; Karam, L. Study of the Resistance of *Staphylococcus aureus* Biofilm, Biofilm-Detached Cells, and Planktonic Cells to Microencapsulated Carvacrol Used Alone or Combined with Low-pH Treatment. *Int. J. Mol. Sci.* **2024**, *25*, 7222. [\[CrossRef\]](#)
- Puentes, E.; Tapia-Perdomo, V.; Espinosa-Valbuena, D.; Reyes Reyes, M.; Quintero-Santander, D.; Vasquez-Dallos, S.; Salazar, H.; Santamaría-Galvis, P.; Silva-Rodríguez, R.; Castillo Villamizar, G. Microbiologically influenced corrosion: The gap in the field. *Front. Environ. Sci.* **2022**, *10*, 924842. [\[CrossRef\]](#)
- Brauer, J.I.; Makama, Z.; Bonifay, V.; Aydin, E.; Kaufman, E.D.; Beech, I.B.; Sunner, J. Mass spectrometric metabolomic imaging of biofilms on corroding steel surfaces using laser ablation and solvent capture by aspiration. *Biointerphases* **2015**, *10*, 019003. [\[CrossRef\]](#)
- Liu, S.; Zhao, C.; Huang, H. Research Progress of Intelligent Anti-Corrosion Coatings and Their Healing Agents. *Adv. Mater. Technol.* **2025**, *10*, 2401669. [\[CrossRef\]](#)
- Enning, D.; Garrelfs, J. Corrosion of iron by sulfate-reducing bacteria: New views of an old problem. *Appl. Environ. Microbiol.* **2014**, *80*, 1226–1236. [\[CrossRef\]](#)
- Yan, M.; Wei, B.; Xu, J.; Li, Y.; Hu, Y.; Cai, Z.; Sun, C. Insight into sulfate-reducing bacteria corrosion behavior of X80 pipeline steel welded joint in a soil solution. *J. Mater. Res. Technol.* **2023**, *24*, 5839–5863. [\[CrossRef\]](#)
- Salgar-Chaparro, S.; Lepkova, K.; Pojtanabuntoeng, T.; Darwin, A.; Machuca, L. Microbiologically influenced corrosion as a function of environmental conditions: A laboratory study using oilfield multispecies biofilms. *Corros. Sci.* **2020**, *169*, 108595. [\[CrossRef\]](#)

19. Wasim, M.; Djukic, M.B. Long-term external microbiologically influenced corrosion of buried cast iron pipes in the presence of sulfate-reducing bacteria (SRB). *Eng. Fail. Anal.* **2020**, *115*, 104657. [\[CrossRef\]](#)
20. Yin, K.; Liu, H.; Cheng, Y.F. Microbiologically influenced corrosion of X52 pipeline steel in thin layers of solution containing sulfate-reducing bacteria trapped under disbonded coating. *Corros. Sci.* **2018**, *145*, 271–282. [\[CrossRef\]](#)
21. Javed, M.A.; Neil, W.C.; McAdam, G.; Wade, S. Effect of sulphate-reducing bacteria on the microbiologically influenced corrosion of ten different metals using constant test conditions. *Int. Biodeterior. Biodegrad.* **2017**, *125*, 75–83. [\[CrossRef\]](#)
22. Javaherdashti, R. Impact of sulphate-reducing bacteria on the performance of engineering materials. *Appl. Microbiol. Biotechnol.* **2011**, *91*, 1507–1517. [\[CrossRef\]](#)
23. Abdus Samad, U.; Alam, M.A.; Anis, A.; Sherif, E.M.; Al-Mayman, S.I.; Al-Zahrani, S.M. Effect of Incorporated ZnO Nanoparticles on the Corrosion Performance of SiO(2) Nanoparticle-Based Mechanically Robust Epoxy Coatings. *Materials* **2020**, *13*, 3767. [\[CrossRef\]](#)
24. Șomoghi, R.; Semenescu, A.; Pasăre, V.; Chivu, O.R.; Nițoi, D.F.; Marcu, D.F.; Florea, B. The Impact of ZnO Nanofillers on the Mechanical and Anti-Corrosion Performances of Epoxy Composites. *Polymers* **2024**, *16*, 2054. [\[CrossRef\]](#)
25. Liu, P.; Zhang, H.; Fan, Y.; Xu, D. Microbially Influenced Corrosion of Steel in Marine Environments: A Review from Mechanisms to Prevention. *Microorganisms* **2023**, *11*, 2299. [\[CrossRef\]](#)
26. Rasheed, P.A.; Jabbar, K.A.; Rasool, K.; Pandey, R.P.; Sliem, M.H.; Helal, M.; Samara, A.; Abdullah, A.M.; Mahmoud, K.A. Controlling the biocorrosion of sulfate-reducing bacteria (SRB) on carbon steel using ZnO/chitosan nanocomposite as an eco-friendly biocide. *Corros. Sci.* **2019**, *148*, 397–406. [\[CrossRef\]](#)
27. Azam, A.; Ahmed, A.S.; Oves, M.; Khan, M.S.; Habib, S.S.; Memic, A. Antimicrobial activity of metal oxide nanoparticles against Gram-positive and Gram-negative bacteria: A comparative study. *Int. J. Nanomed.* **2012**, *7*, 6003–6009. [\[CrossRef\]](#) [\[PubMed\]](#)
28. Houskova, V.; Stengl, V.; Bakardjieva, S.; Murafa, N.; Kalendova, A.; Oplustil, F. Zinc oxide prepared by homogeneous hydrolysis with thioacetamide, its destruction of warfare agents, and photocatalytic activity. *J. Phys. Chem. A* **2007**, *111*, 4215–4221. [\[CrossRef\]](#) [\[PubMed\]](#)
29. Reis, M.A.M.; Almeida, J.S.; Lemos, P.C.; Carrondo, M.J.T. Effect of hydrogen sulfide on growth of sulfate reducing bacteria. *Biotechnol. Bioeng.* **1992**, *40*, 593–600. [\[CrossRef\]](#) [\[PubMed\]](#)
30. Ismail, M.; Yahaya, N.; Bakar, A.A.; Noor, N.N.N. Cultivation of sulphate reducing bacteria in different media. *Malays. J. Civ. Eng.* **2014**, *26*, 456–465. [\[CrossRef\]](#)
31. Ghazy, E.; Mahmoud, M.; Asker, M.; Mahmoud, M.; Abo Elsoud, M.; Abdel Sami, M. Cultivation and detection of sulfate reducing bacteria (SRB) in sea water. *J. Am. Sci.* **2011**, *7*, 604–608.
32. Narkiewicz, U.; Sibera, D.; Kuryliszyn-Kudelska, I.; Kilański, L.; Dobrowolski, W.; Romčević, N. Synthesis by Wet Chemical Method and Characterization of Nanocrystalline ZnO Doped with Fe₂O₃. *Acta Phys. Pol. A* **2008**, *113*, 1695–1700. [\[CrossRef\]](#)
33. Somasiri, M.; Amandani, T.; Basnayaka, C.; Ahsan, A.; Dilangani, G.P.; Herath, A.C.; Bandara, S.; Kyazze, G.; Fernando, E.Y. Direct synthesis of nanomaterials on carbon microfibre electrode material for superior electrocatalysis in lake sediment microbial fuel cells. *Energy Nexus* **2024**, *13*, 100280. [\[CrossRef\]](#)
34. Basnayaka, C.; Somasiri, M.; Ahsan, A.; Nazeer, Z.; Thilini, N.; Bandara, S.; Fernando, E.Y. Marine Photosynthetic Microbial Fuel Cell for Circular Renewable Power Production. *BioEnergy Res.* **2024**, *17*, 2299–2310. [\[CrossRef\]](#)
35. Tamura, K.; Nei, M. Estimation of the number of nucleotide substitutions in the control region of mitochondrial DNA in humans and chimpanzees. *Mol. Biol. Evol.* **1993**, *10*, 512–526. [\[CrossRef\]](#)
36. Nei, M.; Kumar, S. *Molecular Evolution and Phylogenetics*; Oxford university press: Oxford, UK, 2000.
37. Felsenstein, J. Confidence limits on phylogenies: An approach using the bootstrap. *Evolution* **1985**, *39*, 783–791. [\[CrossRef\]](#) [\[PubMed\]](#)
38. Saitou, N.; Nei, M. The neighbor-joining method: A new method for reconstructing phylogenetic trees. *Mol. Biol. Evol.* **1987**, *4*, 406–425. [\[CrossRef\]](#) [\[PubMed\]](#)
39. Gascuel, O. BIONJ: An improved version of the NJ algorithm based on a simple model of sequence data. *Mol. Biol. Evol.* **1997**, *14*, 685–695. [\[CrossRef\]](#) [\[PubMed\]](#)
40. Tamura, K.; Nei, M.; Kumar, S. Prospects for inferring very large phylogenies by using the neighbor-joining method. *Proc. Natl. Acad. Sci. USA* **2004**, *101*, 11030–11035. [\[CrossRef\]](#)
41. Kumar, S.; Stecher, G.; Suleski, M.; Sanderford, M.; Sharma, S.; Tamura, K. MEGA12: Molecular Evolutionary Genetic Analysis version 12 for adaptive and green computing. *Mol. Biol. Evol.* **2024**, *41*, msae263. [\[CrossRef\]](#)
42. Vakilipour Takaloo, A. Corrosion Behavior of Heat Treated Nickel-Aluminum Bronze Alloy in Artificial Seawater. *Mater. Sci. Appl.* **2011**, *02*, 1542–1555. [\[CrossRef\]](#)
43. Sahai, A.; Goswami, N. Structural and vibrational properties of ZnO nanoparticles synthesized by the chemical precipitation method. *Phys. E Low-Dimens. Syst. Nanostructures* **2014**, *58*, 130–137. [\[CrossRef\]](#)
44. Kimuya, A. The modified OHM'S law and its implications for electrical circuit analysis. *Eurasian J. Sci. Eng. Technol.* **2023**, *4*, 59–70. [\[CrossRef\]](#)

45. ASTM G1-03; Standard Practice for Preparing, Cleaning, and Evaluating Corrosion Test Specimens. ASTM International: West Conshohocken, PA, USA, 2017.
46. Zaafarany, I. Cyclic Voltammetric Behavior of Iron Electrode in Sodium Hydroxide Solutions. *Mater. Sci. Res. India* **2009**, *6*, 241–250. [[CrossRef](#)]
47. Hassan Basri, H.; Talib, R.A.; Sukor, R.; Othman, S.H.; Ariffin, H. Effect of Synthesis Temperature on the Size of ZnO Nanoparticles Derived from Pineapple Peel Extract and Antibacterial Activity of ZnO-Starch Nanocomposite Films. *Nanomaterials* **2020**, *10*, 1061. [[CrossRef](#)]
48. Yang, H.; Zhang, J.; Li, Z.; Huang, J.; Wu, J.; Zhang, Y.; Ge, H.; Zhao, Y. Antibacterial Effect of Low-Concentration ZnO Nanoparticles on Sulfate-Reducing Bacteria under Visible Light. *Nanomaterials* **2023**, *13*, 2033. [[CrossRef](#)]
49. Yu, S.; Lou, Y.; Zhang, D.; Zhou, E.; Li, Z.; Du, C.; Qian, H.; Xu, D.; Gu, T. Microbiologically influenced corrosion of 304 stainless steel by nitrate reducing *Bacillus cereus* in simulated Beijing soil solution. *Bioelectrochemistry* **2020**, *133*, 107477. [[CrossRef](#)]
50. Wang, J.; Li, X.; Guan, F.; Yang, Z.; Zhai, X.; Zhang, Y.; Tang, X.; Duan, J.; Xiao, H. The Isolation of Anaerobic and Facultative Anaerobic Sulfate-Reducing Bacteria (SRB) and a Comparison of Related Enzymes in Their Sulfate Reduction Pathways. *Microorganisms* **2023**, *11*, 2019. [[CrossRef](#)]

Disclaimer/Publisher’s Note: The statements, opinions and data contained in all publications are solely those of the individual author(s) and contributor(s) and not of MDPI and/or the editor(s). MDPI and/or the editor(s) disclaim responsibility for any injury to people or property resulting from any ideas, methods, instructions or products referred to in the content.